Check for updates

Received: 15 December 2022 | Revised: 19 March 2023 | Accepted: 26 March 2023

DOI: 10.1002/dep2.230

The Depositional Record
A journal of the International Association of Sedimentologists
Open Access
IAS
WILEY

ORIGINAL RESEARCH ARTICLE

The mechanisms and drivers of lithification in slag-dominated artificial ground

John M. MacDonald[1] | Connor V. Brolly[1] | Charlotte Slaymark[1] | Liene Spruženiece[1] | Claire Wilson[2] | Robin Hilderman[1]

[1]School of Geographical and Earth Sciences, University of Glasgow, Glasgow, G12 8QQ, UK

[2]School of Chemistry, University of Glasgow, Glasgow, G12 8QQ, UK

Correspondence
John M. MacDonald, School of Geographical and Earth Sciences, University of Glasgow, Glasgow G12 8QQ, UK.
Email: john.macdonald.3@glasgow.ac.uk

Funding information
University of Glasgow

Abstract

Unconsolidated artificial ground is an ever-increasing feature on the Earth's surface but it poses various challenges such as pollutant release and ground instability. The process of lithification could be an important factor in changing the properties of artificial ground and ameliorating these challenges. In this study, a lithified deposit of a furnace slag associated with a former iron and steel works in Scotland was analysed to determine the mechanisms and drivers of lithification. Scanning electron microscope analysis showed that Ca leached from around the edges of clasts of slag through reaction of the chemically unstable slag with water from an adjacent water body. Dissolution of Ca (and OH^-) from the slag caused the water in contact with the slag to become hyperalkaline, facilitating ingassing and hydroxylation of CO_2 from the atmosphere (fingerprinted through carbon isotope analysis). Reaction of the dissolved Ca and CO_2 led to precipitation of calcite. Scanning electron microscope analysis showed the calcite is distributed between slag clasts, forming rims around clasts and cementing clasts together into a solid rock-like mass. Understanding the mechanisms and drivers of lithification in artificial ground will be important, given its widespread nature particularly in urban areas where artificial ground is the substrate of most development.

KEYWORDS

artificial ground, calcite, cementation, lithification, slag

1 | INTRODUCTION

The Anthropocene is a proposed geological epoch encompassing significant human impact on the Earth (Waters et al., 2016; Zalasiewicz et al., 2019). In a geological and geomorphological context, humans are agents in sculpting the landscape and creating artificial ground (McMillan & Powell, 1999; Price et al., 2011). Examples of artificial ground deposited by humans on the Earth's surface range from excavated natural rock, such as spoil from deep mining, to anthropogenically-created materials such as steelmaking process wastes (Ford et al., 2014; Price et al., 2011; Riley et al., 2020). Given that worldwide annual anthropogenic shift of sediment is estimated to be *ca* 316 Gt (Cooper et al., 2018), greatly exceeding that of transport by rivers to the oceans (*ca* 11.3 Gt) (Syvitski et al., 2022),

This is an open access article under the terms of the Creative Commons Attribution License, which permits use, distribution and reproduction in any medium, provided the original work is properly cited.
© 2023 The Authors. *The Depositional Record* published by John Wiley & Sons Ltd on behalf of International Association of Sedimentologists.

lithification of artificial ground will play a major role in creating the rocks of the future.

Artificial ground poses a variety of challenges. Many types of artificial ground are unsuitable for building foundations due to their physical properties (Morales, 1993) while the unconsolidated nature of artificial ground can lead to devastating mass movement (e.g. failure of colliery spoil tips; Siddle et al., 1996). Artificial ground will often contain toxic chemicals (e.g. metals, hydrocarbons; Dai et al., 2022; Hobson et al., 2017; Matern et al., 2020), or lead to secondary pollution of surrounding watercourses (e.g. acid mine drainage from colliery spoil; Simate & Ndlovu, 2014). However, artificial ground can present opportunities too. 'Brownfield' land—underlain by artificial ground—is frequently reused for construction and development (Hammond et al., 2021). Due to its varied chemical and physical properties, artificial ground can enhance biodiversity within an area (Macgregor et al., 2022). Artificial ground with a moderate to high calcium content can also potentially be used as CO_2 sinks (Riley et al., 2020; Washbourne et al., 2015). Given these challenges and opportunities, it is important to understand the evolution of the physical and chemical properties of artificial ground. Understanding this is also timely given ever-expanding volumes of artificial ground (Cooper et al., 2018; McMillan & Powell, 1999; Price et al., 2011) and political focus on repurposing land underlain by artificial ground for development (CPRE, 2020; Hammond et al., 2021).

One such potential physical and chemical change is lithification. Artificial ground is typically unconsolidated when deposited, composed of loose material of a wide range of composition and source—anything from construction and demolition waste to colliery spoil to furnace slag to municipal waste. Lithification represents consolidation and fusing together of the loose particles making up the artificial ground through physical and chemical changes. Lithification is a ubiquitous natural process which results in conversion of unconsolidated sediment into sedimentary rock. While lithification is a natural process, it can be anthropogenically induced in soils/sediments. Laboratory experiments indicate that injection of CO_2 into certain types of artificial ground deposits (ultramafic mine tailings) can lead to cementation and stabilisation (Power et al., 2021). While not strictly lithification, microbially induced calcite precipitation (MICP) through harnessing of soil bacteria can be used to stabilise soils and sediments and improve their geochemical properties (Liu et al., 2021; Moravej et al., 2018; Tiwari et al., 2021).

Artificial ground can have a very wide range of compositions. This study documents and investigates lithification of an artificial ground deposit dominated by furnace slag. Slag is the by-product of smelting in a furnace to extract metal(s) from ore. Iron and steel-making slags are composed mainly of calcium silicate minerals, along with aluminates and iron-rich phases (Pullin et al., 2019). They are a voluminous and widespread type of artificial ground—*ca* 0.5 Gt of steelmaking slag is produced globally every year (USGS, 2018), which could reach *ca* 2 Gt year^{-1} by the end of the century (Renforth, 2019). In addition to new slag, there is an estimated 160 million m^3 of legacy slag in the UK alone (Riley et al., 2020), as well as large but unquantified volumes globally, stockpiled or dumped from historical steelmaking. These slags are chemically reactive, undergoing weathering reactions with water and CO_2 (Mayes et al., 2018).

The aim of this paper is to investigate mechanisms and drivers of lithification in slag-dominated artificial ground. Samples from a case study slag heap were analysed to document the microstructures, mineralogy and chemistry of the materials, and to determine the mineralogical and chemical changes during lithification.

2 | MATERIALS AND METHODS

Samples were collected for analysis from an area of artificial ground associated with the former Glengarnock Steelworks in North Ayrshire, Scotland (Figure S1A). Historical maps indicate this area to have been a 'slag works' (Figure S1B), where slag from the furnace will have been stockpiled; there is an estimated *ca* 3.2 km^3 of slag at this site (Riley et al., 2020). Modern geological maps confirm the area is presently underlain by artificial ground (Figure S1C). Although largely capped with soil and vegetated since steelworks closure in the 1970s (McCrone, 1991), field inspection along the north-western shore of Kilbirnie Loch (a freshwater lake) confirms the land surface is underlain with slag. The slag is visible on the lake shore but does not manifest as loose particles (as most slag heaps do); instead it typically appears as a single mass with a hard mid-pale grey or cream-coloured top surface, giving the appearance of a rock made of clasts (Figure 1A).

Three samples (GG1a, GG4 and GG5) were taken from this rocky surface at 55.753359, −4.666098 for further analysis. Inspection of the material shows a breccia-like material, with dark grey clasts of porous slag cemented together by a paler material (Figure 1B) like that on the top surface. Some of this cream-coloured material was scraped off the outer surface of sample GG5 and identified by powder X-ray diffraction (XRD) using a Rigaku MiniFlex 6G equipped with a D/teX Ultra detector, a 6-position (ASC-6) sample changer and Cu sealed tube (Kα1 and Kα2 wavelengths—1.5406 and 1.5444 Å, respectively). Phase identification was carried out with reference to the Crystallographic Open Database.

20554877, 2023, 4, Downloaded from https://onlinelibrary.wiley.com/doi/10.1002/dep2.230 by Nes, Edinburgh Central Office, Wiley Online Library on [23/01/2024]. See the Terms and Conditions (https://onlinelibrary.wiley.com/terms-and-conditions) on Wiley Online Library for rules of use; OA articles are governed by the applicable Creative Commons License

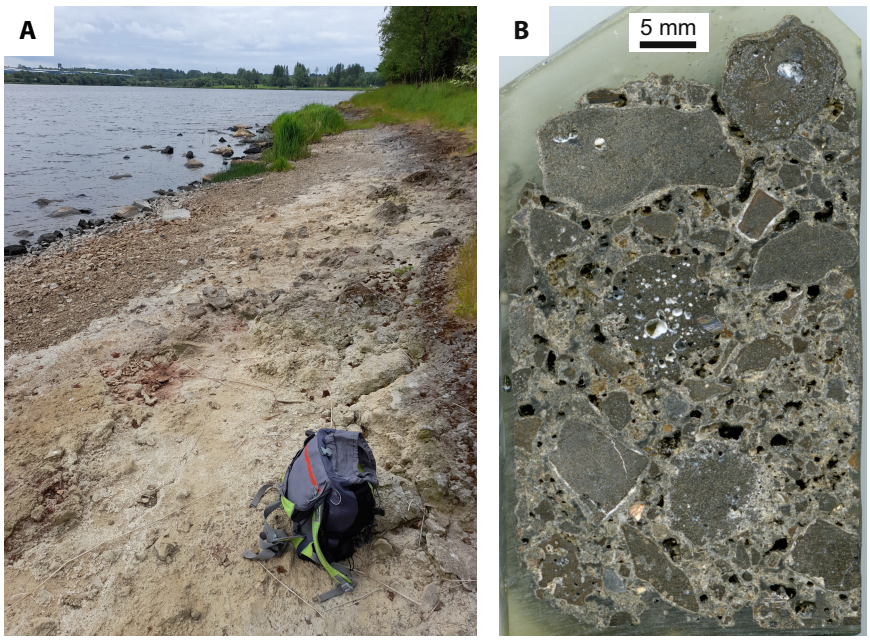

FIGURE 1 (A) Field photograph showing nature of study site with slag fused into a single mass with hard cream-coloured coating on the top surface (70 cm tall rucksack for scale). (B) Cut face of sample showing breccia-like texture—clasts of slag (dark grey) with coatings and interconnecting network of paler cream-coloured material.

A powdered sample of the cream-coloured material from GG5 was analysed for stable carbon and oxygen isotopes. Values of $\delta^{13}C$ and $\delta^{18}O$ were obtained on 200 µg of sample by continuous flow isotope ratio mass spectrometry in the School of Geographical and Earth Sciences at the University of Glasgow. Powder was drilled from the surface and acidified using phosphoric acid (≥1.90 SG) and heated for 1 h at 60°C on an Elementar GasBench and analysed on an Isoprime 100 mass spectrometer. The sample was run in triplicate and the average reported as the result with 1 standard deviation. Values are calibrated to Vienna-Pee Dee Belemnite (V-PDB) using NBS-18 and IAEA-603 reference standards. A secondary standard, IA-RO22 (Iso-Analytical Ltd.) was used to validate the calibration linearity for more depleted values of $\delta^{13}C$ and $\delta^{18}O$ than the reference standards have. Analytical uncertainties of 0.36‰ on $\delta^{13}C$ and 0.75‰ on $\delta^{18}O$ were obtained on measurements of IAEA-603 ($n = 20$) measured during the analytical batch (Table S1).

Sample imaging and chemical mapping was conducted on polished thin sections with a *ca* 20 nm carbon coating using a Zeiss Sigma variable pressure field-emission-gun scanning electron microscope (VP-FEGSEM) equipped with an Oxford Instruments Ultimax 170 mm^2 Silicon Drift Detector Energy dispersive detector, based in the geoanalytical electron microscopy and spectroscopy (GEMS) facility at the University of Glasgow. Backscattered electron (BSE) imaging and energy-dispersive X-ray spectroscopy (EDX) were conducted in high vacuum using high current mode and accelerating voltage of 20 kV, working distance of 8.0 mm and aperture of 60 µm. The EDX mapping data were acquired and processed using the Oxford Instrument AZtec software. All EDX maps shown have had the AZtec true map function applied, that removes background and artefacts, and resolves issues with element peak overlaps.

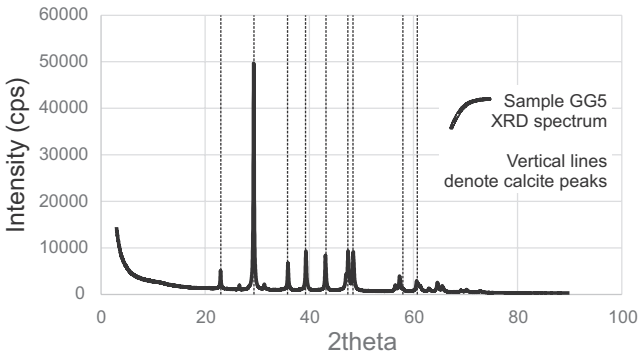

FIGURE 2 XRD spectrum for cream-coloured material coating and fusing together slag pieces, and found on the top surface of the material mass. Note all major peaks in the sample spectra are matched by calcite peaks, indicating the cream-coloured material is dominated by calcite.

3 | RESULTS

At the case study site at Glengarnock, occasional loose pieces of grey slag can be observed at the rock shore but typically exposure of the slag indicates a single rock-like mass with a cream-coloured top surface. Some of this cream-coloured material from sample GG5 was analysed for XRD which showed it to be dominated by calcite (Figure 2). To determine the source of the CO_2 in the calcite of the cream-coloured material, a powder sample of the calcite was analysed for stable carbon and oxygen

20554877, 2023, 4, Downloaded from https://onlinelibrary.wiley.com/doi/10.1002/dep2.230 by Nes, Edinburgh Central Office, Wiley Online Library on [23/01/2024]. See the Terms and Conditions (https://onlinelibrary.wiley.com/terms-and-conditions) on Wiley Online Library for rules of use; OA articles are governed by the applicable Creative Commons License

isotopes, recording a $\delta^{13}C$ value of −20.19 ± 0.23‰ and a $\delta^{18}O$ of −11.97 ± 0.71‰ (Table S1).

The SEM analysis of multiple areas across the three samples showed a similar range of microstructures and element distributions. Six large area BSE images and EDX maps were collected from the three samples; two are shown here (Figures 3 and 4) while the others are included in Figure S2 to further support the observations and interpretations made in this study. In each figure, BSE images (part A) show textural and mineralogical relationships allowing easy distinction between slag clasts and the material in between the clasts (intraclast calcite cement). Calcium and Si maps (parts B and C, respectively) show spatial distribution of those elements within clasts, and between the clasts and the intraclast material, allowing interpretation of mineral phases. Finally, a composite BSE image and EDX map (part D) shows multi-element spatial distribution, again allowing interpretation of mineral phases. The EDX spectra extracted from the maps to indicate phase composition are also presented, in Figures S3–S6.

The dominant component of the samples are the clasts of slag material. The SEM backscatter imaging (Figures 3A and 4A) shows clasts of slag with a polycrystalline texture, indicated by variable greyscale (in BSE) and heterogeneous distribution of Ca (Figures 3B and 4B) and Si (Figures 3C and 4C) within the clasts, suggesting multiple phases within the slag. Clasts vary in size, from >20 mm in diameter to fragments <10 μm across. Clast shape is typically irregular and angular to sub-angular, although some perfectly rounded clasts are found. Internally, slag clasts are polycrystalline, with crystal shape ranging from circular to acicular, rounded to angular and often irregular (Figures 3A and 4A). Crystal size is highly variable, ranging from *ca* 1 μm or less to hundreds of microns in diameter. Circular, or irregular but rounded, crystals are bright (in BSE) and rich in Fe (Figures 3D and 4D). These are Mg-Fe-Mn oxides and are present throughout the slag clasts. In some slag clasts, Fe-rich and Mg-rich crystals exhibit zoning, with Fe higher around the crystal edges and Mg concentrated in the cores (Figure 3D). The Fe-bearing and Mg-bearing crystals within the slag clasts are variable in size, from *ca* 1 μm or less to *ca* 100 μm. Other crystals within the slag clasts are typically calcium silicates, with variable proportions of Ca and Si reflecting different mineralogies. Acicular crystals present in some slag clasts are composed of calcium iron aluminates or calcium phosphates. At the clast scale, some slag clasts exhibit a higher concentration overall of Ca in the cores of the clasts, with narrow Ca-poor rims around the edges of the clasts (Figure 3B).

Some other non-polycrystalline clasts are present. Mainly, these are dominated by Si, that is quartz (Figure 3D). These are equant in shape, with some up to

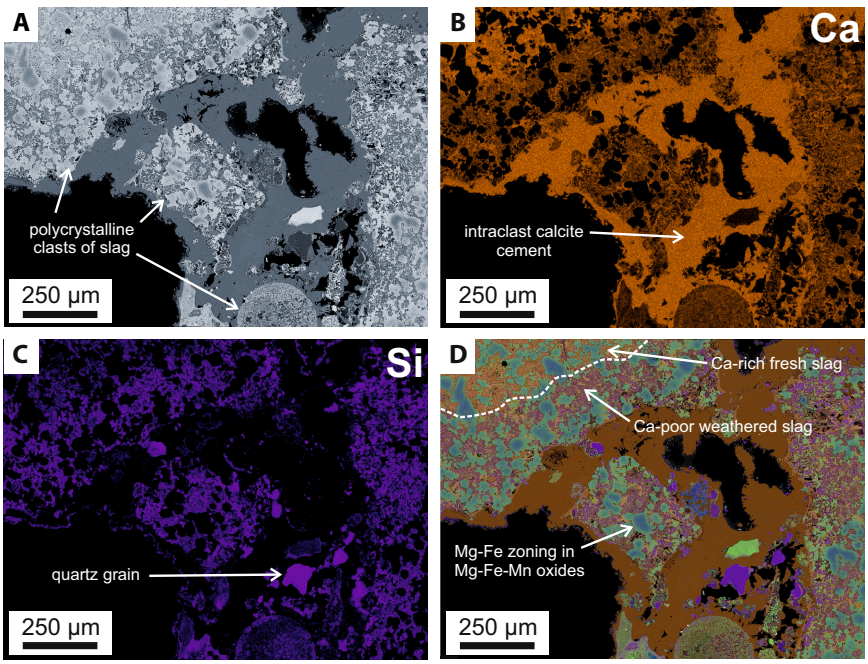

FIGURE 3 SEM analysis of microstructures. (A) BSE image showing polycrystalline texture slag clasts. (B) EDX map showing distribution of Ca in same area as the BSE map—note intense Ca in the intraclast material (calcite cement). (C) EDX map showing distribution of Si in same area as the BSE map—note the occasional detrital quartz grain. (D) Composite BSE image and EDX map (orange = Ca; purple = Si; green = Fe; dark blue = Mg)—note only Ca found in intraclast material (calcite cement), relative difference in Ca and Si between the core and rim of some slag clasts (denoting slag weathering), and core-edge zoning of Fe and Mg in some crystals.

20554877, 2023, 4, Downloaded from https://onlinelibrary.wiley.com/doi/10.1002/dep2.230 by Nes, Edinburgh Central Office, Wiley Online Library on [23/01/2024]. See the Terms and Conditions (https://onlinelibrary.wiley.com/terms-and-conditions) on Wiley Online Library for rules of use; OA articles are governed by the applicable Creative Commons License

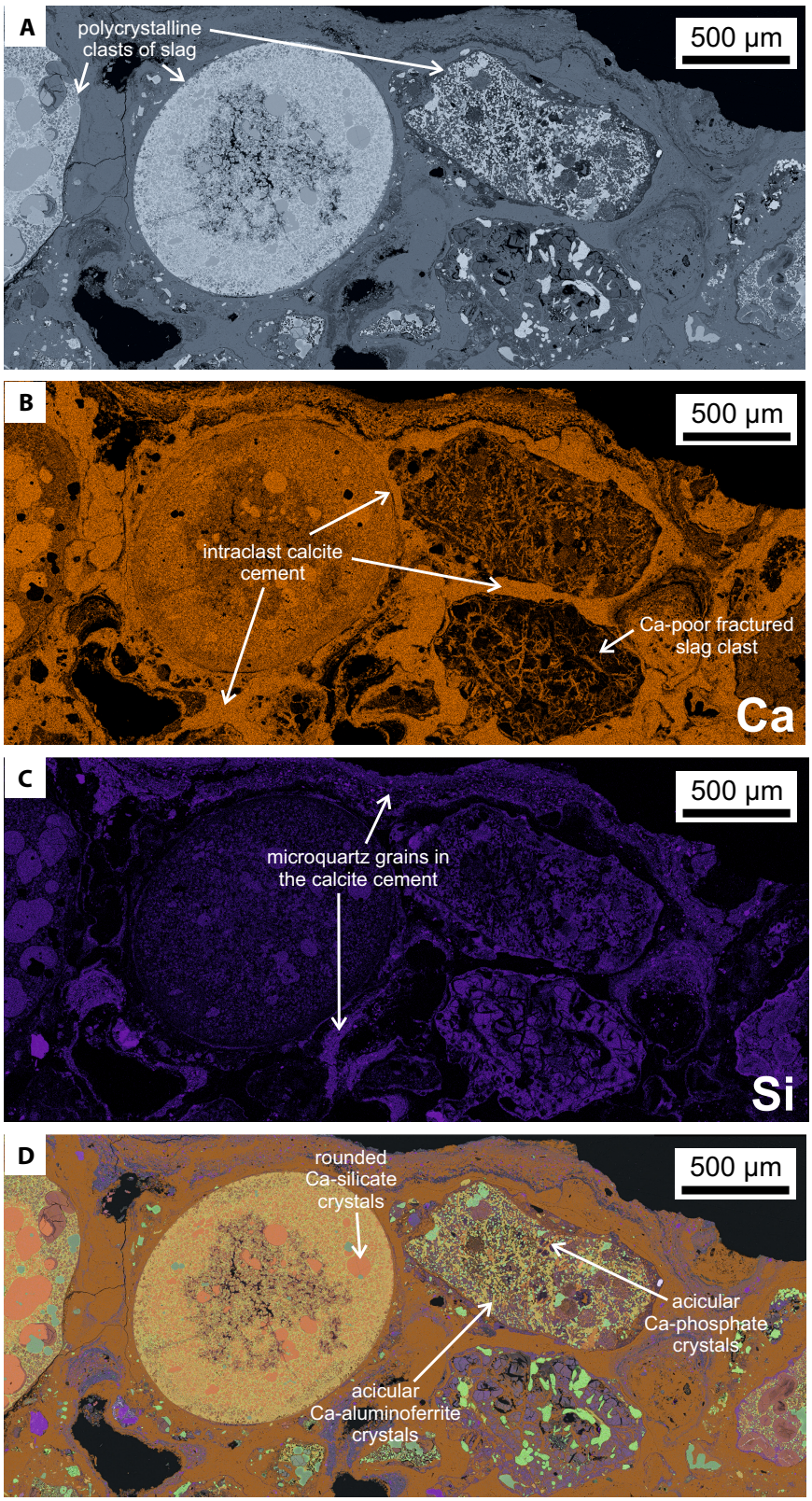

FIGURE 4 SEM analysis of microstructures. (A) BSE image showing polycrystalline texture slag clasts. (B) EDX map showing distribution of Ca in same area as the BSE map—note variable Ca intensity within and between slag clasts (e.g. Ca-poor fractured clast), and uniformly high Ca intensity in intraclast material (calcite cement). (C) EDX map showing distribution of Si in same area as the BSE map—note general absence of Si from intraclast material apart from patches with bands of microquartz parallel to clast/surface edges. (D) Composite BSE image and EDX map (orange = Ca; purple = Si; green = Fe)—note Ca dominating intraclast material (calcite), and variable distribution of Fe, Si and Ca picking out different minerals and crystal shapes within the slag clasts, including acicular calcium phosphate and calcium aluminoferrite, and rounded forms of Ca-silicate.

ca 100 µm in diameter, but they mainly occur as very small grains, occurring as bands in among the material between the slag clasts (Figure 4C). These smaller grains may be accumulations of detrital microquartz trapped during the formation of the intraclast material.

The intraclast material forms a network around the slag clasts, with rims around the clasts joining together and leaving little pore space. Apart from some layering, BSE images do not show crystal shape within this material due to the uniform grey colour. However, at the interface

20554877, 2023, 4, Downloaded from https://onlinelibrary.wiley.com/doi/10.1002/dep2.230 by Nes, Edinburgh Central Office, Wiley Online Library on [23/01/2024]. See the Terms and Conditions (https://onlinelibrary.wiley.com/terms-and-conditions) on Wiley Online Library for rules of use; OA articles are governed by the applicable Creative Commons License

with pore spaces, some crystal shapes can be viewed, often showing at least a partial bladed or prismatic habit. The intraclast material is dominated by Ca (Figures 3B and 4B); EDX spectra show it is a calcium carbonate—the calcite identified in the XRD analysis.

4 | DISCUSSION

4.1 | Mechanism of lithification

Historical map evidence indicates the area of artificial ground studied is a slag heap and visual inspection during fieldwork confirmed the ground was dominated by slag. The slag heap would have originally been composed of loose clasts of slag but it has now been partly lithified, at least at the surface where the samples were taken from. The SEM-BSE imaging (Figures 3A and 4A) confirms the present material consists dominantly of clasts of slag (polycrystalline, consisting of calcium-silicates, calcium phosphate, calcium aluminoferrite and Mg-Fe-Mn oxides) with minor clasts of detrital quartz sand. In all samples, the EDX mapping shows that the clasts are cemented together with a Ca-rich (no Si or Fe, or other metals) phase (Figures 3B and 4B); XRD confirms this phase to be calcite. The EDX mapping shows that many of the slag clasts have a zone of lower Ca around the edge, compared to the core of the clasts (Figures 3B,D and 4B,D), while Si remains consistent between core and edge (Figures 3C and 4C). This indicates leaching of Ca from the edges of many of the slag clasts, with precipitation of the calcite cement being the destination for the leached Ca. Hobson et al. (2017) noted a similar narrow zone of Ca leaching at the edge of a piece of slag, in this case with a thin rim of calcite on the slag surface. While that study showed a calcite rim on a single piece of slag, and this study documents calcite cementation and lithification of multiple slag clasts, the mechanism of Ca leaching and resulting calcite precipitation is the same. Calcium is leached from the slag clasts when they come into contact with water, as in Equation (1; Mayes et al., 2018; Pullin et al., 2019):

$$Ca_2SiO_4 + 4H_2O \rightarrow 2Ca^{2+} + H_4SiO_4 + 4OH \quad (1)$$

In Equation (1), OH^- anions are produced as well as Ca, causing a rise in pH. Mayes et al. (2018) documented this in the Howden Burn, a stream with a pH of >11 draining a slag heap at Consett in north-east England. The resulting highly alkaline nature of water in contact with the slag clasts promotes ingassing and hydroxylation of atmospheric CO_2 which then reacts with the dissolved Ca (leached from the slag) to precipitate calcite (Mayes et al., 2018). The strongly negative $\delta^{13}C$ value recorded at Glengarnock of $-20.05 \pm 0.23‰$ validates the source as being atmospheric CO_2. Hydroxylation and instant calcite precipitation would give a $\delta^{13}C$ value of *ca* −25 to −27‰ (Dietzel et al., 1992; Falk et al., 2016; Renforth et al., 2009). The fact that the $\delta^{13}C$ is slightly less depleted than this end member value, but still strongly negative, indicates minor influence on the $\delta^{13}C$ value from another process. The combined $\delta^{13}C$ and $\delta^{18}O$ values of $-20.05 \pm 0.23‰$ and $-12.05 \pm 0.72‰$, respectively plot in the DIC (dissolved inorganic carbon) equilibration field of Falk et al. (2016), who measured carbon and oxygen isotopes in calcites in an analogous hyperalkaline setting of springs in the Semail ophiolite in Oman. The isotopic ratios recorded in this study indicate that there was minor DIC equilibration of ingassed and hydroxylated CO_2 in the water on the slag at Glengarnock prior to calcite precipitation. Similarly, in the tufa at Consett, the $\delta^{13}C$ values did not reflect end member hydroxylation, instead indicating mixing between hydroxylation and biogenic carbon inputs (with an end member of *ca* −8‰ Cerling, 1984). This reflected the fact that calcite precipitation occurred tens to hundreds of metres from the source of the Ca in a stream with scope for introduction of biogenic carbon (Renforth et al., 2009). At Glengarnock, where calcite precipitation is in situ on the slag itself, there is limited or no scope for input of biogenic carbon, hence the interpretation of minor DIC equilibration after hydroxylation of atmospheric CO_2. The BSE imaging and EDX mapping presented here (Figures 3 and 4) show that this same process of ingassing and hydroxylation of atmospheric CO_2 can lead to precipitation of large enough volumes of calcite to act as a cement and lithify numerous clasts of slag together.

4.2 | Drivers of lithification

The calcite cement is the key component in the lithification of the slag-dominated artificial ground in this study. Thin coatings and pore linings of calcite have been observed on slag surfaces by the authors and in the studies of Hobson et al. (2017) and Khudhur et al. (2022) but these are much smaller volumes than those documented in the slag heap at Glengarnock in this study. The driver for initiating the process of calcite precipitation is water (Equation 1), and the slag samples in the studies of Hobson et al. (2017) and Khudhur et al. (2022) appear only to have had thin films of moisture/rainwater on the surfaces where Ca was leached and calcite precipitated. In the tufa in the Howden Burn, a much larger volume of calcite was precipitated as the volume of water in the stream facilitated greater leaching of Ca from the Consett slag heap, resulting in the large volume of tufa precipitated in

20554877, 2023, 4, Downloaded from https://onlinelibrary.wiley.com/doi/10.1002/dep2.230 by Nes, Edinburgh Central Office, Wiley Online Library on [23/01/2024]. See the Terms and Conditions (https://onlinelibrary.wiley.com/terms-and-conditions) on Wiley Online Library for rules of use; OA articles are governed by the applicable Creative Commons License

the stream bed, downstream from the slag heap (Mayes et al., 2018; Renforth et al., 2009).

At Glengarnock, the volume of calcite precipitated as cement in the slag heap is large relative to the studies of Hobson et al. (2017) and Khudhur et al. (2022), although not at the same scale as the Howden Burn tufa. In common with that site though is the presence of a large volume of water, in this case Kilbirnie Loch. The position of the lithified portion of the slag heap—along the lake shore (Figure 1A)—suggests that the lake water was a key driver in leaching Ca from the slag (Equation 1) and the resulting calcite cement precipitation. Historical evidence indicates that Kilbirnie Loch is approximately a third smaller than on the first edition Ordnance Survey map due to being filled in with slag from the steelworks (McCrone, 1991), leading to ample time for slag and water to interact. Since slag dumping and processing ended around 1980, fluctuating lake levels will have resulted in ongoing infiltration of lake water into the slag at the lake shore, refreshing the source of water in Equation 1, allowing Ca (and OH^-) leaching to proceed. Lake water washed by wave action onto the shore and caught in little ponds on the rough surface of the slag heap (Figure 1A) will have been isolated enough from the diluting effect of the lake so as to become hyperalkaline, allowing CO_2 ingassing and hydroxylation and ultimately calcite precipitation. In the case of the Howden Burn at Consett, the flow of stream water (*ca* 2–10 L/s, Mayes et al., 2018) is low enough to still allow for hyperalkalinity in the stream. Similarly in the streams and springs in the Semail ophiolite have low enough flow rates not to be too dilute for the interaction of the water and rock to lead to hyperalkalinity (Clark et al., 1992; Falk et al., 2016; Mervine et al., 2014). The presence of the calcite as a cement in among the slag clasts indicates that lake water has percolated into the slag heap along the lake shore and has been present in large enough concentration to leach enough Ca and ingas and hydroxylate enough CO_2 to precipitate the calcite cement but in low enough concentrations as to not dilute the hyperalkalinity—the key factor in facilitating the calcite precipitation and cementation. This process is summarised in the conceptual model in Figure 5.

Artificial ground, specifically made ground deposited on the natural land surface by humans, is typically unconsolidated in nature. Much of it is composed of particles of natural rock excavated and dumped by human activity, for example colliery spoil, or anthropogenic mineral materials, for example furnace slags. Such artificial ground can pose various challenges, ranging from pollution to ground instability. Precipitation of a calcite cement has been shown to stabilise soils and sediments (Power et al., 2021; Stocks-Fischer et al., 1999), and therefore, the occurrence of this process in unstable slag heaps can

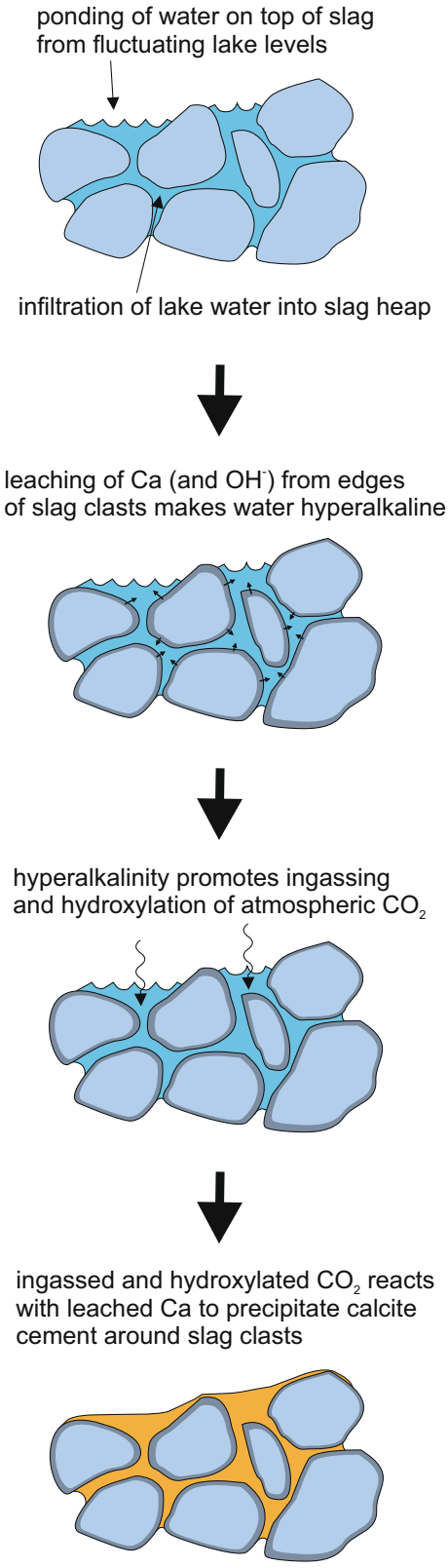

FIGURE 5 Conceptual model of the lithification process.

be important in reducing the risk of failure and harm to humans. Precipitated calcite can also immobilise potentially toxic metals (Merrikhpour & Jalali, 2012; Olsson et al., 2014a, 2014b), which are likely to be present in

20554877, 2023, 4, Downloaded from https://onlinelibrary.wiley.com/doi/10.1002/dep2.230 by Nes, Edinburgh Central Office, Wiley Online Library on [23/01/2024]. See the Terms and Conditions (https://onlinelibrary.wiley.com/terms-and-conditions) on Wiley Online Library for rules of use; OA articles are governed by the applicable Creative Commons License

higher concentrations in artificial ground than in the natural environment. In the slag-dominated artificial ground studied here, the lithification through the precipitation of calcite will minimise the risk of pollution and ground instability. Some artificial ground types are excavated and reused, such as furnace slags for aggregate or as a cement substitute (Renforth, 2019) and lithification of any such deposits may influence how easy they are to excavate.

Artificial ground can also present opportunities as well as challenges. In slag-dominated artificial ground in particular, the source of Ca in a readily weathered material can facilitate drawdown and mineralisation of CO_2 from the atmosphere. The precipitation of calcite in the lithification of the slag heap documented in this study has drawn down atmospheric CO_2 (as shown by the $\delta^{13}C$ analysis) which has been mineralised, thus illustrating the potential for the lithification process to also contribute to atmospheric CO_2 reduction targets.

The sheer volume of artificial ground (Cooper et al., 2018; Price et al., 2011) means that it may become a key component of future rocks. Rocks created through lithification of artificial ground have some similarities to natural sedimentary rocks, such as being composed of clasts and lithified with mineral cement, but are also markedly different given the anthropogenic influence on their formation. The clasts can be made of anthropogenically deposited artificial ground—anything from colliery spoil to municipal waste to the furnace slag in this study—which have become naturally lithified, in this study through atmospheric CO_2 drawdown and leaching of Ca from clasts of anthropogenically created furnace slag. Plastiglomerate—natural beach rocks cemented together with anthropogenically melted plastic (Corcoran et al., 2014)—are another form of anthropogenic rock, but the form of anthropogenic rock described here—clasts of anthropogenic material (artificial ground) cemented together naturally—have greater potential to form the rocks of the future due to the large volumes of artificial ground present globally.

5 | CONCLUSIONS

Unconsolidated artificial ground is an ever-increasing feature on the Earth's surface and lithification could be an important factor in changing its physical properties. In this study, a lithified portion of a furnace slag deposit associated with a former iron and steel works was analysed to determine the mechanisms and drivers of lithification. Scanning electron microscope imaging and chemical mapping showed that Ca leached from around the edges of clasts of slag through the reaction of the chemically unstable slag and water from the adjacent lake. Dissolution of Ca (and OH^-) from the slag caused the water in contact with the slag to become hyperalkaline, which facilitated ingassing and hydroxylation of atmospheric (fingerprinted from carbon isotope analysis) CO_2. Reaction of dissolved Ca and CO_2 led to precipitation of calcite (identified by XRD). The SEM analysis showed that calcite is distributed in between the slag clasts, forming rims around clasts and cementing clasts together into a solid rock-like mass.

Anthropogenically derived rocks such as this may be widespread but so far undocumented, with cementation and lithification of artificial ground facilitated by chemical reactions involving an in situ anthropogenic material (in this instance ingassed and hydroxylated atmospheric CO_2 reacting with Ca leached from the slag). Similarly, natural sediments, for example river gravels, may become cemented and lithified by calcite formed by the same mechanism with Ca leached and transported from an ex situ anthropogenic mineral source of Ca such as furnace slag, fly ash or paper mill waste. With ever-increasing volumes of artificial ground, particularly in urban areas, lithification could ameliorate some of the challenges posed by artificial ground, such as reducing the risk of slope failure and immobilising pollutants. Given this, understanding the mechanisms and drivers of naturally-occurring lithification in artificial ground of a range of mineral and chemical compositions presents an important avenue for future research.

ACKNOWLEDGEMENTS

The analysis in this paper was partly funded by a COVID recovery grant from the University of Glasgow to J.M.M. North Ayrshire Council are thanked for facilitating access and sampling. Colin Waters and another anonymous reviewer are thanked for their constructive and positive reviews, as well as associate editor Benjamin Walter for prompt editorial handling.

CONFLICT OF INTEREST STATEMENT

The authors declare that they have no known competing financial interests or personal relationships that could have appeared to influence the work reported in this paper.

DATA AVAILABILITY STATEMENT

The data that supports the findings of this study are available in the supplementary material of this article.

ORCID

John M. MacDonald https://orcid.org/0000-0002-8609-804X

REFERENCES

Cerling, T.E. (1984) The stable isotopic composition of modern soil carbonate and its relationship to climate. *Earth and Planetary Science Letters*, *71*, 229–240.

20554877, 2023, 4, Downloaded from https://onlinelibrary.wiley.com/doi/10.1002/dep2.230 by Nes, Edinburgh Central Office, Wiley Online Library on [23/01/2024]. See the Terms and Conditions (https://onlinelibrary.wiley.com/terms-and-conditions) on Wiley Online Library for rules of use; OA articles are governed by the applicable Creative Commons License

Clark, I.D., Fontes, J.-C. & Fritz, P. (1992) Stable isotope disequilibria in travertine from high pH waters: laboratory investigations and field observations from Oman. *Geochimica et Cosmochimica Acta*, *56*, 2041–2050.

Cooper, A.H., Brown, T.J., Price, S.J., Ford, J.R. & Waters, C.N. (2018) Humans are the most significant global geomorphological driving force of the 21st century. *The Anthropocene Review*, *5*, 222–229.

Corcoran, P.L., Moore, C.J. & Jazvac, K. (2014) An anthropogenic marker horizon in the future rock record. *GSA Today*, *24*, 4–8.

CPRE (2020) Recycling our land: the state of brownfield 2020. *9*.

Dai, C., Han, Y., Duan, Y., Lai, X., Fu, R., Liu, S., Leong, K.H., Tu, Y. & Zhou, L. (2022) Review on the contamination and remediation of polycyclic aromatic hydrocarbons (PAHs) in coastal soil and sediments. *Environmental Research*, *205*, 112423.

Dietzel, M., Usdowski, E. & Hoefs, J. (1992) Chemical and 13C/12C- and 18O/16O-isotope evolution of alkaline drainage waters and the precipitation of calcite. *Applied Geochemistry*, *7*, 177–184.

Falk, E.S., Guo, W., Paukert, A.N., Matter, J.M., Mervine, E.M. & Kelemen, P.B. (2016) Controls on the stable isotope compositions of travertine from hyperalkaline springs in Oman: insights from clumped isotope measurements. *Geochimica et Cosmochimica Acta*, *192*, 1–28.

Ford, J.R., Price, S.J., Cooper, A.H. & Waters, C.N. (2014) An assessment of lithostratigraphy for anthropogenic deposits. *Geological Society, London, Special Publications*, *395*, 55–89.

Hammond, E.B., Coulon, F., Hallett, S.H., Thomas, R., Hardy, D., Kingdon, A. & Beriro, D.J. (2021) A critical review of decision support systems for brownfield redevelopment. *Science of the Total Environment*, *785*, 147132.

Hobson, A.J., Stewart, D.I., Bray, A.W., Mortimer, R.J.G., Mayes, W.M., Rogerson, M. & Burke, I.T. (2017) Mechanism of vanadium leaching during surface weathering of basic oxygen furnace steel slag blocks: a microfocus X-ray absorption spectroscopy and electron microscopy study. *Environmental Science & Technology*, *51*, 7823–7830.

Khudhur, F.W.K., Macente, A., MacDonald, J.M. & Daly, L. (2022) Image-based analysis of weathered slag for calculation of transport properties and passive carbon capture. *Microscopy and Microanalysis*, *28*, 1–12.

Liu, J., Li, G. & Xa, L. (2021) Geotechnical engineering properties of soils solidified by microbially induced $CaCO_3$ precipitation (MICP). *Advances in Civil Engineering*, *2021*, 6683930.

Macgregor, C.J., Bunting, M.J., Deutz, P., Bourn, N.A.D., Roy, D.B. & Mayes, W.M. (2022) Brownfield sites promote biodiversity at a landscape scale. *Science of the Total Environment*, *804*, 150162.

Matern, K., Weigand, H., Kretzschmar, R. & Mansfeldt, T. (2020) Leaching of hexavalent chromium from young chromite ore processing residue. *Journal of Environmental Quality*, *49*, 712–722.

Mayes, W.M., Riley, A.L., Gomes, H.I., Brabham, P., Hamlyn, J., Pullin, H. & Renforth, P. (2018) Atmospheric CO_2 sequestration in iron and steel slag: Consett, County Durham, United Kingdom. *Environmental Science & Technology*, *52*, 7892–7900.

McCrone, G. (1991) Urban renewal: the Scottish experience. *Urban Studies*, *28*, 919–938.

McMillan, A.A. & Powell, J.H. (1999) Classification of artificial (man-made) ground and natural superficial deposits––applications to geological maps and datasets in the UK. BGS Rock Classification Scheme Keyworth, British Geological Survey, 4.

Merrikhpour, H. & Jalali, M. (2012) Waste calcite sludge as an adsorbent for the removal of cadmium, copper, lead, and zinc from aqueous solutions. *Clean Technologies and Environmental Policy*, *14*, 845–855.

Mervine, E.M., Humphris, S.E., Sims, K.W.W., Kelemen, P.B. & Jenkins, W.J. (2014) Carbonation rates of peridotite in the Samail Ophiolite, Sultanate of Oman, constrained through 14C dating and stable isotopes. *Geochimica et Cosmochimica Acta*, *126*, 371–397.

Morales, E.M. (1993) Structural and functional distress due to slag expansion. Third International Conference on Case Histories in Geotechnical Engineering, St Louis, MO.

Moravej, S., Habibagahi, G., Nikooee, E. & Niazi, A. (2018) Stabilization of dispersive soils by means of biological calcite precipitation. *Geoderma*, *315*, 130–137.

Olsson, J., Stipp, S.L.S. & Gislason, S.R. (2014a) Element scavenging by recently formed travertine deposits in the alkaline springs from the Oman Semail Ophiolite. *Mineralogical Magazine*, *78*, 1479–1490.

Olsson, J., Stipp, S.L.S., Makovicky, E. & Gislason, S.R. (2014b) Metal scavenging by calcium carbonate at the Eyjafjallajökull volcano: a carbon capture and storage analogue. *Chemical Geology*, *384*, 135–148.

Power, I.M., Paulo, C., Long, H., Lockhart, J.A., Stubbs, A.R., French, D. & Caldwell, R. (2021) Carbonation, cementation, and stabilization of ultramafic mine tailings. *Environmental Science & Technology*, *55*, 10056–10066.

Price, S.J., Ford, J.R., Cooper, A.H. & Neal, C. (2011) Humans as major geological and geomorphological agents in the Anthropocene: the significance of artificial ground in Great Britain. *Philosophical Transactions of the Royal Society A: Mathematical, Physical and Engineering Sciences*, *369*, 1056–1084.

Pullin, H., Bray, A.W., Burke, I.T., Muir, D.D., Sapsford, D.J., Mayes, W.M. & Renforth, P. (2019) Atmospheric carbon capture performance of legacy iron and steel waste. *Environmental Science & Technology*, *53*, 9502–9511.

Renforth, P. (2019) The negative emission potential of alkaline materials. *Nature Communications*, *10*, 1401.

Renforth, P., Manning, D.A.C. & Lopez-Capel, E. (2009) Carbonate precipitation in artificial soils as a sink for atmospheric carbon dioxide. *Applied Geochemistry*, *24*, 1757–1764.

Riley, A.L., MacDonald, J.M., Burke, I.T., Renforth, P., Jarvis, A.P., Hudson-Edwards, K.A., McKie, J. & Mayes, W.M. (2020) Legacy iron and steel wastes in the UK: extent, resource potential, and management futures. *Journal of Geochemical Exploration*, *219*, 106630.

Siddle, H.J., Wright, M.D. & Hutchinson, J.N. (1996) Rapid failures of colliery spoil heaps in the South Wales Coalfield. *Quarterly Journal of Engineering Geology*, *29*, 103–132.

Simate, G.S. & Ndlovu, S. (2014) Acid mine drainage: challenges and opportunities. *Journal of Environmental Chemical Engineering*, *2*, 1785–1803.

Stocks-Fischer, S., Galinat, J.K. & Bang, S.S. (1999) Microbiological precipitation of $CaCO_3$. *Soil Biology and Biochemistry*, *31*, 1563–1571.

Syvitski, J., Ángel, J.R., Saito, Y., Overeem, I., Vörösmarty, C.J., Wang, H. & Olago, D. (2022) Earth's sediment cycle during the Anthropocene. *Nature Reviews Earth & Environment*, *3*, 179–196.

Tiwari, N., Satyam, N. & Sharma, M. (2021) Micro-mechanical performance evaluation of expansive soil biotreated with

20554877, 2023, 4, Downloaded from https://onlinelibrary.wiley.com/doi/10.1002/dep2.230 by Nes, Edinburgh Central Office, Wiley Online Library on [23/01/2024]. See the Terms and Conditions (https://onlinelibrary.wiley.com/terms-and-conditions) on Wiley Online Library for rules of use; OA articles are governed by the applicable Creative Commons License

indigenous bacteria using MICP method. *Scientific Reports*, *11*, 10324.

USGS. (2018) USGS minerals yearbook 2018.

Washbourne, C.L., Lopez-Capel, E., Renforth, P., Ascough, P.L. & Manning, D.A.C. (2015) Rapid removal of atmospheric CO_2 by urban soils. *Environmental Science & Technology*, *49*, 5434–5440.

Waters, C.N., Zalasiewicz, J., Summerhayes, C., Barnosky, A.D., Poirier, C., Gałuszka, A., Cearreta, A., Edgeworth, M., Ellis, E.C., Ellis, M., Jeandel, C., Leinfelder, R., McNeill, J.R., Richter, D., Steffen, W., Syvitski, J., Vidas, D., Wagreich, M., Williams, M., Zhisheng, A., Grinevald, J., Odada, E., Oreskes, N. & Wolfe, A.P. (2016) The Anthropocene is functionally and stratigraphically distinct from the Holocene. *Science*, *351*, aad2622.

Zalasiewicz, J., Waters, C.N., Williams, M. & Summerhayes, C.P. (2019) *The Anthropocene as a geological time unit: a guide to the scientific evidence and current debate*. Cambridge: Cambridge University Press.

SUPPORTING INFORMATION

Additional supporting information can be found online in the Supporting Information section at the end of this article.

How to cite this article: MacDonald, J. M., Brolly, C. V., Slaymark, C., Spruženiece, L., Wilson, C. & Hilderman, R. (2023). The mechanisms and drivers of lithification in slag-dominated artificial ground. *The Depositional Record*, *9*, 810–819. https://doi.org/10.1002/dep2.230

20554877, 2023, 4, Downloaded from https://onlinelibrary.wiley.com/doi/10.1002/dep2.230 by Nes, Edinburgh Central Office, Wiley Online Library on [23/01/2024]. See the Terms and Conditions (https://onlinelibrary.wiley.com/terms-and-conditions) on Wiley Online Library for rules of use; OA articles are governed by the applicable Creative Commons License